Frequency analysis of dopant profiling and capacitance spectroscopy using Scanning Microwave Microscopy

Enrico Brinciotti[a], Giulio Campagnaro[a], Giorgio Badino[a], Manuel Kasper[a], Georg Gramse[b], Silviu Sorin Tuca[b], Juergen Smoliner[c], Thomas Schweinboeck[d], Soeren Hommel[d], and Ferry Kienberger[a,*]

[a] Keysight Technologies Austria GmbH, Keysight Labs, Gruberstrasse 40, 4020 Linz, Austria
[b] Johannes Kepler University, Biophysics Institute, Gruberstrasse 40, 4020 Linz, Austria
[c] Technical University of Vienna, Institute of Solid State Electronics, Floragasse 7, 1040 Vienna, Austria
[d] Infineon Technologies, Failure Analysis, Am Campeon 1-12, 85579 Neubiberg, Germany
[*] Correspondence: ferry_kienberger@keysight.com

***Abstract*— Broadband dS_{11}/dV dopant profiling at GHz frequencies and *in situ* calibrated Capacitance-Voltage spectroscopy of silicon p-n junctions using Scanning Microwave Microscopy (SMM) are reported. Using a 3D finite element model to obtain the E-field distribution at the tip/sample interface, we show that the reflected S_{11} signal is expected to vary monotonically with the doping concentration. S_{11} imaging performed on two doped silicon samples confirms the simulation results for the full SMM operating frequency range of 1-20 GHz. In this frequency range we compare the S_{11} data with the differential dS_{11}/dV data commonly used for dopant profiling. In standard SMM operating conditions the S_{11} data is monotonic over the full frequency range of 1-20 GHz, while the dS_{11}/dV data shows a monotonic dependence on the doping concentration between 10^{14} and 10^{20} atoms/cm^3 only at lower frequencies. A non-monotonic behavior is observed at higher frequencies. This is important for the frequency selection of dS_{11}/dV for dopant profiling applications. We also show S_{11} based calibrated capacitance measurements and capacitance-voltage curves of differently doped sample regions and of p-n junction interfaces.**

Keywords*— *scanning microwave microscopy, dopant profiling, nanoscale, microwave, semiconductors

I. INTRODUCTION

Scanning Microwave Microscopy (SMM) allows characterizing electric and magnetic properties of materials at microwave frequencies with nanometer lateral resolution [1-9]. SMM merges the nanoscale imaging of an atomic force microscope (AFM) with the high-frequency broadband (from MHz to GHz) impedance measurement capabilities of a vector network analyzer (VNA). The typical frequency range of the combined SMM is between 1-20 GHz. In reflection SMM mode, the ratio of the reflected and incident electromagnetic waves, the so called S_{11} scattering parameter, is measured by the VNA at each AFM tip/sample contact point. There are two main different imaging modes in SMM. The first is quantitative dopant profiling by means of dS_{11}/dV, which is a widely used technique for semiconductor failure analysis and detecting leakages in solid state devices with nanometers resolution. For quantitative measurements, a dopant calibration sample is required to convert the differential dS_{11}/dV data into doping concentrations [10, 20]. The dS_{11}/dV mode relies on a low frequency (kHz) modulation of the GHz S_{11} signal that allows tuning the semiconductor depletion zone and probing the doping concentration through the native oxide interface. The dS_{11}/dV signal is not affected by the so called topographic cross-talk, therefore it gives immediate information that only depends on the material properties and is not influenced by topographical features of the sample. The second SMM mode is complex impedance imaging and it is based directly on the scattering S_{11} signal [11-15]. The S_{11} signal is detected by the VNA and depends on the tip-sample relative electrical impedance and on contributions coming from the transmission line cables and RF connectors. A de-embedding process is therefore necessary to convert the raw S_{11} into a calibrated S_{11} that depends only on the complex impedance between tip and sample. Several complex impedance calibration procedures have been developed in the past [11-12, 16-17]. We used an impedance calibration workflow developed recently [12], that requires no calibration sample, allowing an *in situ* calibration directly on the sample under test. While the dS_{11}/dV mode works also for samples with rough topographies, the topography-crosstalk needs to be filtered out in complex impedance S_{11} imaging [13]. As such, S_{11} imaging works particularly well for nearly flat samples with small topography features.

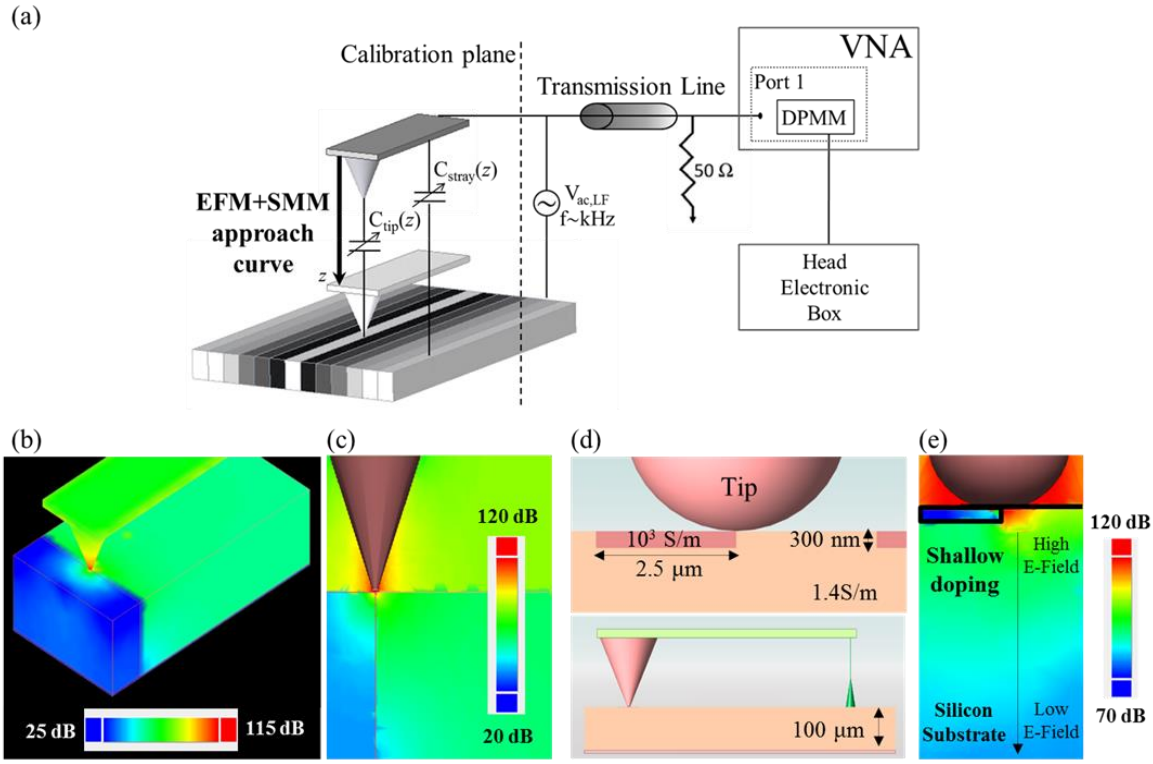

Figure 1. (a) SMM measurement sketch for simultaneous topography, S_{11} and dS_{11}/dV measurements. (b) 3D E-field distribution of the tip-sample system done with EM-Pro modeling. The E-field is lower in the doped region with high-conductivity (shown in blue), than in the Si bulk of the sample (shown in green). (c) Cross-section of the 3D E-field distribution. (d) EM-Pro model geometry (bottom), with a zoom on the shallow doped structure (top). The shallow stripes are 300 nm high, 2.5 µm wide, with a conductivity of 10^3 S/m. The silicon bulk is modeled with a conductivity of 1.4 S/m. (e) Cross-section of the E-field distribution showing the tip-sample region. The E-Field is highest close to the tip and decreases inside the sample.

In the following we show dopant profiling dS_{11}/dV as well as complex impedance S_{11} measurements on two differently doped silicon samples that have no significant topography, resulting therefore in negligible topographic cross-talk contributions. We compare dopant profiling and complex impedance measurements at different frequencies over a range of doping level from 10^{14} up to 10^{20} atoms per cm^3. Using the complex impedance S_{11} calibration workflow [12], we also show quantitative capacitance-voltage C-V spectroscopy extracting the curves directly from calibrated capacitance images of a p- and n-doped sample with known dopant densities. By applying the same calibration procedure to a p-n junction, we exhibit pointwise C-V curves acquired on both p-doped and n-doped sides of the junction.

II. MATERIALS AND METHODS

A. SMM hardware

A commercial SMM consisting of a Keysight 5600 Atomic Force Microscope (AFM) interfaced with a Keysight E8362B Vector Network Analyzer (VNA) (10 MHz - 20 GHz), was used. Rocky Mountain Nanotechnology (RMN) conductive solid platinum AFM tips with a nominal tip radius of 80 nm and spring constant of 18 N/m were employed (25Pt300B).

Figure 1a shows the SMM setup. A microwave signal (1-20 GHz) is generated by the VNA and sent through a transmission line circuit to the AFM conductive cantilever. The signal travels through a matching network including a half-wavelength resonator coaxial cable and a 50 Ω shunt resistor. This ensures that the GHz electromagnetic wave follows an impedance matched path when travelling from the 50 Ω RF environment to the higher impedance (kΩ) nanometer scale tip/sample system [18]. Depending on the sample's electrical properties, the signal is partly transmitted and partly back-reflected. The same RF path used to feed the sample is used to carry the reflected wave back to the VNA, where the returning signal is compared with a copy of the incident wave and the S_{11} scattering parameter is measured.

B. Samples under test

Two commercially available samples were used. Both are topographically flat doped silicon (Si) samples. The first, produced by IMEC CAMS (Center for Advanced Metrology Solutions, Belgium) [19], consists of five layers of silicon, 5 µm wide, with different dopant density ranging between 3×10^{14} atoms per cm^3 and 2×10^{19} atoms per cm^3. In each doped area the doping depth extends over the full sample depth (i.e. ~1 cm). The wafer is then cleaved to expose the sample for cross-section profile SMM characterization.

The second sample, produced by Infineon Technologies (Failure Analysis Division, Munich) [6, 20], is composed of a p-Si substrate (10^{15} atoms per cm^3) with 10 different n-type and 10 different p-type implant areas, each with 4×10^{15}, $1 \times$

10^{16}, 4×10^{16}, 1×10^{17}, 4×10^{17}, 1×10^{18}, 4×10^{18}, 1×10^{19}, 4×10^{19}, and 1×10^{20} atoms per cm^3. The doped areas in the active region are 2 µm wide and 300 nm deep. Phosphorus and boron implants depth profiling performed on each doped region by means of Secondary Ion Mass Spectrometry (SIMS), not shown here, reveal homogeneous profiles until 300 nm in depth, followed by an exponential decay and a complete drop at roughly 1 µm from the surface. The n-doped and p-doped regions are next to each other and therefore can be imaged in one SMM scan. No further processing or cleaning steps were performed prior to SMM imaging. The Infineon bi-polar sample, unlike the IMEC uni-polar sample, is designed to be imaged in a standard horizontal configuration and not in cross-section.

C. EMPro Simulations

The 3D-field solver EMPro (Keysight Technologies) was used for modeling the E-field and impedance values of the tip-sample system. All the finite element method (FEM) simulations have been performed at 19 GHz. Figure 1b shows a 3D distribution of E-field magnitude at the tip-sample system on the interface between two doped silicon regions having different doping concentrations. This geometry model describes, in a simplified way, the structure of the uni-polar n-type doped calibration sample, where the differently doped regions extend over the entire sample thickness. The E-Field has a maximum, as expected, near the very end of the conductive tip. The part of the sample where the field is low (shown in blue in the color map), corresponds to the region with higher doping concentration. Accordingly, the field is higher (shown in green), in the region with lower conductivity (i.e. lower doping concentration). A 2D cross-section of the 3D E-field distribution is included in Figure 1c.

One of the differences between the bi-polar and the uni-polar dopant calibration samples is that the former presents shallow doped regions which extend only within few hundreds of nanometers from the sample surface, whereas in the latter they extend over the entire sample thickness. For this reason a different CAD geometry has been designed to model the Infineon sample (shown in Figure 1d and 1e). The shallow stripes are 300 nm high and 2.5 µm wide, with a conductivity of 1000 S/m. The silicon bulk is modeled with a conductivity of 1.4 S/m. Figure 1e shows a cross-section of the tip-sample EM interaction. The E-Field has a maximum close to the SMM tip, decreasing proportionally to the depth in the bulk region, whereas it reaches a relative minimum value inside the shallow doped stripe, which is 300-nm thick. The penetration depth of the E-field is roughly half a micrometer into the sample, which is comparable with the doping depth. As such, the shallow doped regions give a signal contrast that allows differentiating them from the below substrate, which is only partly probed by the E-field. If, for instance, the shallow doped layer would have been only 30 nm thick (instead of 300 nm), then a similar E-field distribution would probe a substantial part of the substrate below, thus generating an unwanted convolution of two contributions from different material regions (i.e. shallow highly doped region and lowly doped substrate).

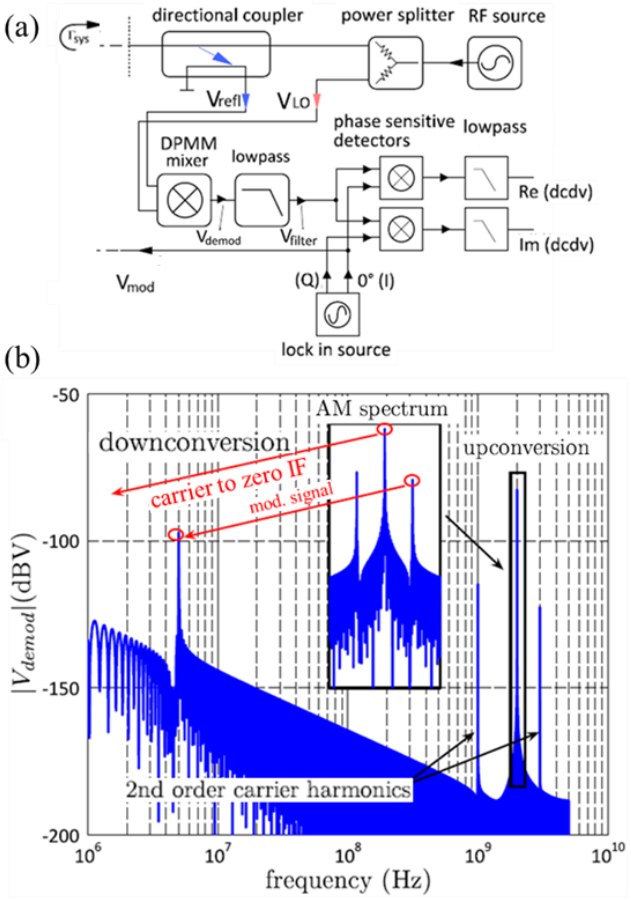

Figure 2. (a) DPMM (dopant profiling measurement module) measurement sketch for dS_{11}/dV measurements. In the differential capacitance measurement mode the reflected S_{11} signal is used as a carrier and a low frequency modulation signal in the kHz range is superimposed to it. (b) DPMM signal spectrum showing the demodulated signal versus frequency. The down-conversion and up-conversion frequency regions show the main harmonic as well as the 2nd order carrier harmonics. An inset shows the AM spectrum of the carrier signal at zero intermediate frequency (IF).

D. dS_{11}/dV imaging for doping profiling

dS_{11}/dV imaging was performed by means of a dopant profiling measurement module (DPMM) attached to the four auxiliary inputs of the VNA and a lock-in modulation technology. The operating principle is explained in details in [10]. Since the technique effectively measures the derivative of the C-V curve with respect to the bias voltage at a fixed DC bias, the *dS_{11}/dV* output signal is also referred to as *dC/dV* signal. Figure 2a shows the measurement setup for *dS_{11}/dV* measurements, which uses the reflected S_{11} signal as a carrier and superimposes to a modulation signal at low frequency (i.e. kHz). The modulation drive signal V_{mod} in the kHz region is created by a synthesized source within the lock-in amplifier and fed to the sample via a bias tee (not drawn). The RF carrier signal (1–20 GHz), is simultaneously sent to the SMM system through a directional coupler. Due to changes in the capacitance of the sample induced by the V_{mod} signal, the reflected V_{refl} signal is modulated at a rate equal to V_{mod}. The signal returned toward the VNA is a superposition of the RF

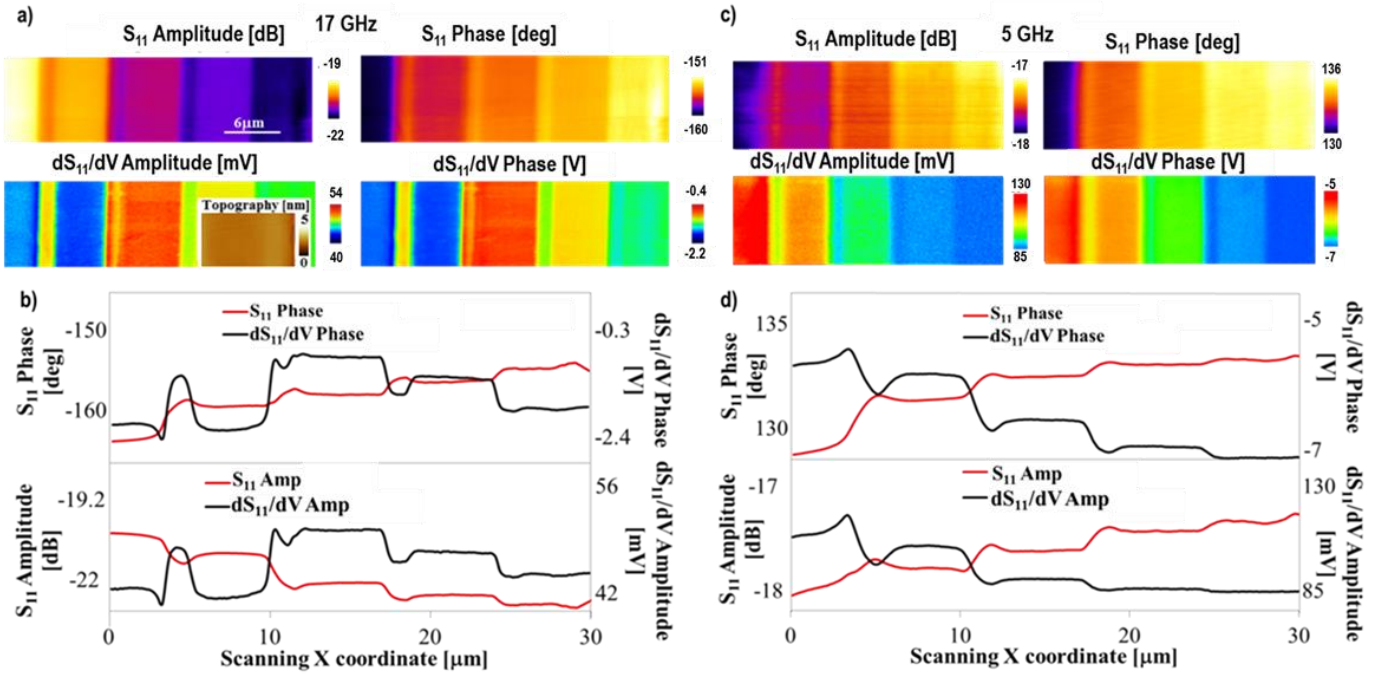

Figure 3. Single polarity n-type doped Si sample imaged with SMM at two different frequencies (left panel 17 GHz, right panel 5 GHz). The sample is a topographically flat staircase structure (see inset in a) consisting of 5 differently doped areas (each wide 5 μm) with doping concentrations increasing (from left to right) from $3x10^{14}$ to $2x10^{19}$ atoms/cm^3 (IMEC, Belgium) All the images have been acquired with a tip DC bias of +0.5V. (a) S_{11} and dS_{11}/dV amplitude and phase at 17GHz. (b) Horizontal cross-section of the dS_{11}/dV and S_{11} phase (top) and amplitude (bottom) images. (c) S_{11} and dS_{11}/dV amplitude and phase at 5GHz. (d) Horizontal cross-section of the dS_{11}/dV and S_{11} phase (top) and amplitude (bottom) images at 5GHz. At 5 GHz, not only the S_{11} amplitude and phase images, but also the dS_{11}/dV amplitude and phase signals show a monotonic behavior over the entire doping range. At higher frequencies (i.e. 17 GHz), S_{11} amplitude and phase signals show a monotonic behavior over the entire doping range, while dS_{11}/dV amplitude and phase signals show a non-monotonic behavior.

signal in the GHz range and the V_{mod} modulation. The directional coupler extracts the reflected signal V_{refl}, which is fed into the DPMM mixer. A direct conversion architecture is used to convert the modulated RF signal V_{refl} into the baseband at zero IF frequency (V_{demod}). For this purpose a balanced mixer is employed and the necessary LO signal (V_{LO}) is extracted by a power splitter directly after the RF source. Figure 2b shows the DPMM signal spectrum of the demodulated signal versus frequency. Once the high frequency RF part of the signal has been removed with a lowpass filter, the V_{filter} signal is sent to a second lock-in amplifier operating at the modulation frequency. The second lock-in amplifier rectifies the V_{filter} signal and generates a DC output signal which is proportional to the modulation response of the capacitance. The complex dS_{11}/dV signal can be interchangeably expressed, keeping the same information, either as amplitude and phase or x- and y-component. Together with the dS_{11}/dV imaging, the DPMM provides a 30 dB amplification of the S_{11} reflected signal. In our experiments the incident microwave power was set to −3 dBm (dBm meaning dB per mW input power), a modulation frequency of 15 kHz and a modulation drive of 0.5V were used.

E. Complex impedance calibration workflow

A calibration procedure [12] was used to convert the S_{11} into calibrated capacitance. The proposed method allows moving the calibration plane of the VNA to the AFM cantilever and works *in situ* on the sample under test. Therefore, the results are not impacted by anything that is located by the upstream end of the tip/sample interface in the SMM system and there is no requirement to use a calibration sample to de-embed the raw-data. The calibration procedure is based on the simultaneous acquisition of Electrostatic Force Microscopy (EFM) and S_{11} approach curves in order to calculate the three error coefficients in a standard S_{11} black box calibration. A low frequency ($\omega=2\pi f=9.42krad/s$, $f = 1.5\ kHz$) EFM approach curve is used to measure the capacitance change with the distance when the cantilever approaches the sample surface. The relation between electrostatic force, F_{es} and tip-sample capacitance, $C(z)$, is:

$$F_{es} = \frac{1}{4}\frac{dC}{dz}V_o^2\cos(2\omega t) \xrightarrow{yields} \frac{dC}{dz} = \frac{2F_{es,2\omega}}{V_o^2} \quad (1)$$

By integration, $C(z)$ is obtained and

$$Z_{in}(z)^{-1} = Y(z) = i2\pi f C(z) \quad (2)$$

From the acquired EFM and S_{11} approach curve, the error parameters (e_{00}, e_{01}, e_{11}), can be calculated from Z_{in} and S_{11}:

$$S_{11,a} = \frac{Z_{in}-Z_{ref}}{Z_{in}+Z_{ref}} \xrightarrow{yields} S_{11,m} = e_{00} + e_{01}\frac{S_{11,a}}{1-e_{11}S_{11,a}} \quad (3)$$

The raw SMM S_{11} data are then converted into capacitance values using the three e-parameters.

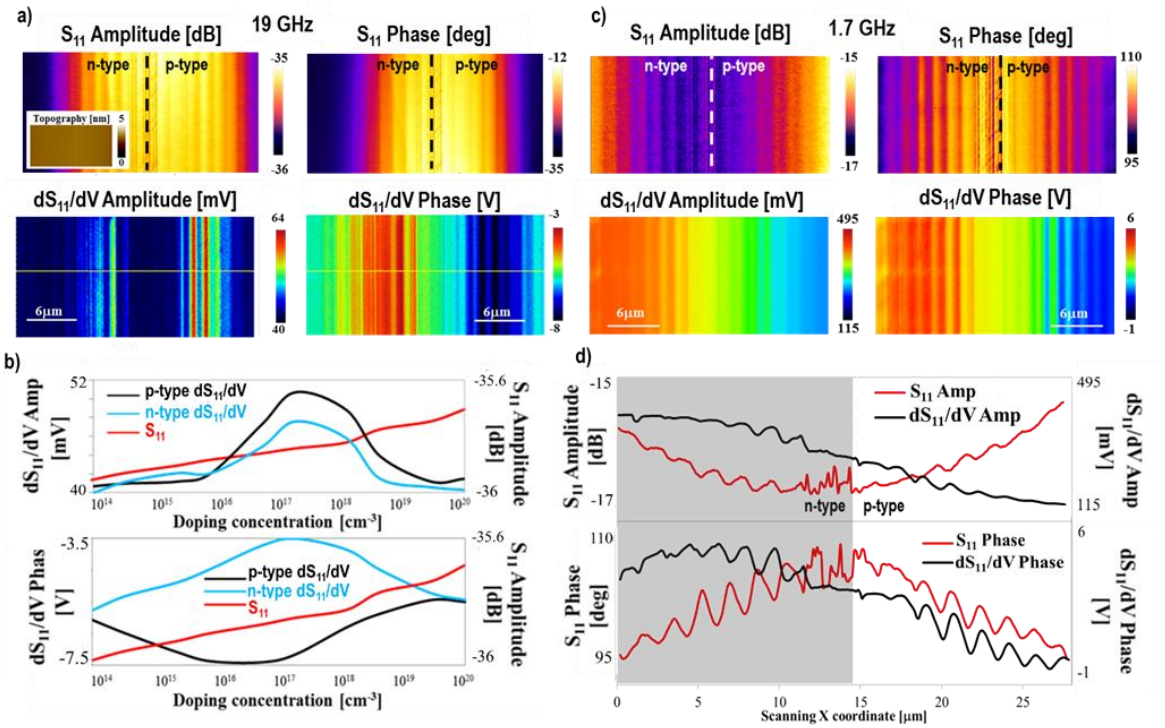

Figure 4. Bipolar n-type and p-type doped Si sample imaged with SMM at two different frequencies (left panel 19 GHz, right panel 1.7 GHz). (a) S_{11} amplitude with flat topography (inset); S_{11} phase; dS_{11}/dV amplitude; dS_{11}/dV phase at 19GHz. The sample is a topographically flat doped Si staircase structure, consisting of 10 n-type and 10 p-type two-µm wide implant areas, with doping concentrations ranging from $4x10^{15}$ to $1x10^{20}$ atoms/cm^3 (Infineon, Germany)(b) Averaged S_{11} amplitude and dS_{11}/dV signals of each doped region plotted versus the doping concentration. While the S_{11} amplitude signal shows a monotonic behavior over the entire doping range, the dS_{11}/dV signal shows a parabolic behavior, with the dS_{11}/dV phase signal revealing the dopant polarity (donor or acceptor). (c) S_{11} amplitude; S_{11} phase; dS_{11}/dV amplitude; dS_{11}/dV phase acquired at 1.7GHz. (d) Horizontal cross-section of the dS_{11}/dV and S_{11} amplitude (top) and phase (bottom) images. At low frequency, not only the S_{11} amplitude and phase images, but also the dS_{11}/dV amplitude and phase signals show a monotonic behavior over the entire doping range.

III. RESULTS AND DISCUSSION

A. S_{11} and dS_{11}/dV frequency dependance

We performed simultaneous S_{11} and dS_{11}/dV imaging at high frequency (17 GHz; Figure 3 left panel) and at low frequency (5 GHz; Figure 3 right panel) on the uni-polar n-doped silicon sample. Amplitude and phase of the complex S_{11} signal detect the regions with different doping densities and monotonically vary with the doping concentration both at 17 GHz and 5 GHz. Also the differential dS_{11}/dV signal provides a clear contrast between the different doping concentrations. At 5 GHz (Figure 3c, d), both amplitude and phase of the complex dS_{11}/dV signal monotonically decrease with the increase of dopant density from left to right. However, looking at the horizontal cross-section profile of Figure 3b, it is easy to notice that the monotonic dependence of the dS_{11}/dV signal on the doping concentration, at 17 GHz, stops at a certain threshold value. This shows that the impedance S_{11} values change monotonically with respect to the dopant density for both high and low frequencies, while the differential dS_{11}/dV is only monotonic over the full doping range at low frequencies.

The same behavior has been observed on the bi-polar doped sample, which includes both n-type and p-type doped silicon regions in a single scan (Figure 4). Also in this case, S_{11} is monotonic over the full doping range for both high (19 GHz) and low (1.7 GHz) frequencies. Again, at lower frequency both dS_{11}/dV amplitude and phase signals change monotonically over the full dopant range (i.e. $4x10^{14}$ atoms/cm^3-10^{20} atoms/cm^3). This is valid for both n-type and p-type doped regions. However, at high frequency the dS_{11}/dV signal presents an inversion of the contrast at a certain doping density and the signal is not monotonic over the full dopant range anymore, as observed also for the uni-polar sample.

SMM quantitative doping profiling is typically performed by acquiring dS_{11}/dV amplitude and phase images of a calibration standard with known doping levels. A calibration curve that correlates the dS_{11}/dV signal to the doping level is thus generated. dS_{11}/dV imaging is then performed on the sample under investigation, and the doping concentration is extracted fitting the results with the calibration curve [10]. However, as shown here, the frequency needs to be adjusted accordingly such that monotonic behavior of dS_{11}/dV versus dopant density is guaranteed. When working in the lower region of the SMM 1-20 GHz frequency range, the acquired dS_{11}/dV signal is found to be directly proportional to the full range of doping concentrations. When working in the high frequency range, the monotonic behavior stops at a particular doping concentration and the calibration is valid only in the corresponding doping range. In between, a gradual transition between the two regimes is observed.

The doping concentration at which the monotonic behavior stops depends both on the frequency and on the tip diameter.

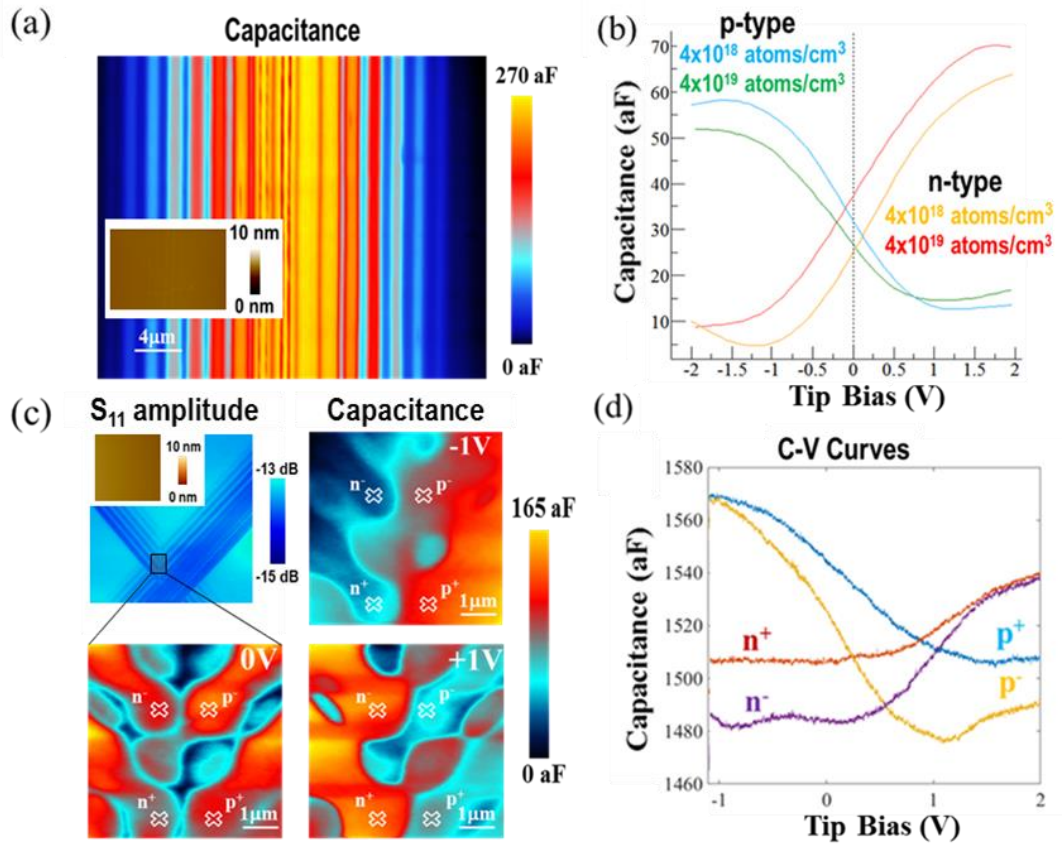

Figure 5. Capacitance-voltage spectroscopy experiments. (a) Calibrated capacitance and topography (inset), of the bipolar doped Si staircase calibration sample with n- and p-implanted areas (Infineon). (b) A DC tip bias voltage has been applied during the scan in a range from -2V to 2V, in steps of 0.5V (AFM tip: RMN 18 N/m, f_{PNA}=19.83GHz). C-V curves generated from vertical cross-sections of the capacitance image show the capability of the SMM to detect the impurity polarity directly from the capacitance image. (c) Wide S_{11} amplitude with topography (inset), and zoomed-in calibrated capacitance of a flat p-n junction structure located on a different area of the Infineon doped Silicon sample. The three capacitance images have been acquired at -1V, 0V, and +1V tip bias, respectively. The capacitance of the n-doped (p-doped) region increases (decreases) when the DC tip bias voltage is increased from -1V to +1V. (d) Pointwise C-V spectroscopy curves in the four different spots labeled with crosses in (c). The curves have been acquired by keeping the tip on the cross labels shown in (c) and by sweeping the tip bias from -1V to +2V in steps of 0.1V.

As proposed in a previous study [21], this frequency dependent behavior can be attributed to the tip-sample interaction physics, in particular to the frequency-dependent depletion capacitance and local surface resistance that control the RC time constant of tip-to-sample interaction. This behavior can be leveraged also to obtain a frequency selective contrast of the dS_{11}/dV at different doping concentrations, as also shown in [21]. Accordingly, the doping concentration value at which the dS_{11}/dV signal exhibits its maximum depends on the selected frequency in the SMM operating range of 1-20 GHz, as shown in [21] and in this paper. This proves particularly useful when a specific doping concentration value needs to be analyzed on the sample under test.

B. Capacitance-voltage spectroscopy on a silicon pn junction

The impedance S_{11} calibration workflow (cf. Materials and Methods section) has been applied to the bi-polar doped silicon sample to obtain calibrated capacitance images at different tip DC-voltage bias. Figure 5a shows the calibrated capacitance image of the differently doped n-type and p-type regions acquired with no tip bias. The capacitance depends on the doping density and reaches up to 300 aF, with high capacitance values observed on highly doped silicon regions. This is in line with the FEM modeling results (Figure 1,b-e), which show how the E-field reaches a relative minimum inside the shallow doped stripe, thus suggesting that more signal is reflected here than in the low doped substrate.

The same region has been imaged by sweeping the DC tip bias between -2V and +2V with steps of 0.3V (data not shown). For both the n-type and p-type stripes an averaged vertical cross-section of two stripes with an impurity concentration of $4x10^{18}$ atoms/cm^3 and $4x10^{19}$ atoms/cm^3, respectively, has been extracted from the capacitance images with different tip bias and plotted in Figure 5b. In this way, the C-V curve is obtained directly from the calibrated capacitance images. The conductive platinum tip and the thin native silicon dioxide layer (~1 nm) with the doped silicon substrate below together form a Metal-Oxide-Semiconductor (MOS) structure. In this configuration, for n-type doped silicon regions, we measured an increase in capacitance at high positive voltages which is in line with the standard depletion zone model [22, 23]. The C–V curve for the p-type stripes shows high capacitance values at negative tip bias and low capacitance at positive tip bias which follows also the textbook model.

A second region of interest on the Infineon sample includes multiple p-n junction structures with doping concentration

values ranging between $4x10^{14}$ atoms/cm^3 and 10^{20} atoms/cm^3. The topography of the area is flat, and the structures are only visible in the electrical images (Figure 5c). Also in this case, the same area has been imaged multiple times in different DC tip bias conditions. The complex impedance calibration workflow has been applied to obtain, from S_{11} amplitude and phase images, calibrated capacitance images of the p-n junction structures (Figure 5c). From the capacitance images the different polarity of the n-type and p-type region can be determined during imaging. When the tip bias is set to -1V, the n-type region shows low capacitance values and the p-type region lights up with a higher capacitance. The exact opposite is true for a tip bias of +1V. By holding the SMM tip in contact with the sample surface in a given position and sweeping the tip DC bias, a pointwise C-V curve can be acquired. In both the n-type and p-type regions, two spots (shown with an *x* in Figure 5c) with different doping concentrations have been chosen and the pointwise C-V experiment has been conducted (Figure 5d). Again the same type of C-V behavior is obtained for the p-type and n-type doping as in Figure 5b. These results show that the C-V curves can be either determined pointwise at particular positions or also from the entire capacitance image acquired at different DC tip-bias voltages.

IV. CONCLUSIONS

An analysis of the frequency dependent contrast mechanism of dopant profiling and impedance SMM is presented. The analysis is based on the assessment of the dS_{11}/dV and S_{11} response at the lower and higher frequency regions of the SMM working range of 1–20 GHz. The impedance S_{11} signal is obtained to be monotonic over the full dopant range for both low and high measurement frequencies. In a previous paper [6], we showed that the impedance S_{11} signal can be used also for quantitative dopant profiling. As such, the S_{11} signal can be used over the entire frequency range from 1-20 GHz for evaluating dopant concentrations. The dS_{11}/dV signal is found to show also a monotonic dependence on the doping concentration but only when operated in lower frequencies. At higher frequencies, a non-monotonic dS_{11}/dV behavior is observed. This is relevant for the dopant profiling dS_{11}/dV calibration procedure. It shows that the measurement frequency needs to be held constant during the calibration workflow when both the dopant calibration sample and the device under test are measured. An impedance S_{11} calibration method has been applied to obtain calibrated capacitance images at different tip DC voltage bias. From the calibrated images, C-V curves on both n-type and p-type regions with different doping concentrations have been obtained. The shape of the C-V curves follows the depletion zone characteristics of doped silicon, which means higher capacitance values at negative tip bias and lower capacitance at positive tip bias for p-type silicon, and the reverse behavior for n-type silicon. The impedance S_{11} calibration workflow has been applied also on a p-n junction structure to obtain capacitance images at different tip bias conditions. The application of different tip-bias allows distinguishing p-type from n-type doping areas. In differently doped spots of the p-n junction structure, pointwise C-V curves have been obtained by keeping the tip in contact with the sample surface while sweeping the tip bias. It shows also that the tip can be positioned with nanometer accuracy between the differently doped areas that have a lateral distance in the range of a micrometer. The results are important for semiconductor dopant calibrations using the differential dS_{11}/dV method, which is commonly used in semiconductor failure analysis labs. Also it shows how reliable C-V spectroscopy data can be acquired during scanning and locally at different lateral positions. Considering the broad range of SMM applications for semiconductor samples, the present work provides a useful overview to choose the most appropriate SMM signal (i.e. dS_{11}/dV or S_{11}), the measurement frequency, as well as the DC tip-bias for reliable and quantitative measurements.

ACKNOWLEDGMENT

We would like to thank Matthias Fenner from Keysight Technologies Germany for the fruitful technical discussions and Prof. Peter Hinterdorfer for the AFM related advices. This work has been supported by EC-FP7 PEOPLE-2012-ITN-317116 Nanomicrowave and Austrian FFG Nanospec 843594.

REFERENCES

[1] Imtiaz A. et al., (2014), Near-field scanning microwave microscopy: An Emerging Research Tool for Nanoscale Metrology, IEEE Microw. Mag. 15 pp. 52–64.

[2] Anlage S. M. et al., (2007), Principles of near-field microwave microscopy. Scanning Probe Microscopy: Electrical and Electromechanical Phenomena at the Nanoscale, vol 1 ed S V Kalinin and A Gruverman (New York: Springer) pp. 215–53 ISBN: 978-0-387-28667-9.

[3] Talanov V. V. et al., (2009), Near-field scanning microwave microscope for interline capacitance characterization of nanoelectronics interconnect, IEEE Trans. MTT 57 1224–9.

[4] Gregory A. et al., (2012), Spatially resolved electrical characterisation of graphene layers by an evanescent field microwave microscope, Physica E 56 431–4.

[5] Vlahacos C. P. et al., (1996), Near-field scanning microwave microscope with 100 μm resolution, Appl. Phys. Lett. 69 3272–4A.

[6] Brinciotti E. et al., (2015), Probing resistivity and doping concentration of semiconductors at the nanoscale using scanning microwave microscopy, Nanoscale, 7, pp. 14715-14722.

[7] Tselev A. et al., (2012), Near-field microwave scanning probe imaging of conductivity inhomogeneities in CVD graphene, Nanotechnology 23 385706 (11pp).

[8] Ma E. Y. et al., (2015), Mobile metallic domain walls in an all-in-all-out magnetic insulator, Science, Vol. 350, Issue 6260, pp. 538-541.

[9] Gao C. et al., (1997), High spatial resolution quantitative microwave impedance microscopy by a scanning tip microwave near-field microscope, Appl. Phys. Lett. 71 1872–4.

[10] H. P. Huber, et al., (2012), Calibrated nanoscale dopant profiling using a scanning microwave microscope, J. Appl. Phys. 111, 014301.

[11] Huber H.P et al., (2010), Calibrated nanoscale capacitance measurements using a scanning microwave microscope, Rev. Sci. Instrum. 81, 113701.

[12] Gramse G. et al., (2014), Calibrated complex impedance and permittivity measurements with Scanning Microwave Microscopy, Nanotechnology 25 8 145703.

[13] Biagi M.C. et al., (2016), Nanoscale Electric Permittivity of Single Bacterial Cells at Gigahertz Frequencies by Scanning Microwave Microscopy, ACS Nano, 10 (1), pp. 280–288.

[14] Tuca S. et al., (2016), Calibrated complex impedance of CHO cells and E. coli bacteria at GHz frequencies using scanning microwave microscopy, Nanotechnology 27 135702 (9pp).

[15] Ren Y. et al., (2015), Direct Imaging of Nanoscale Conductance Evolution in Ion-Gel-Gated Oxide Transistors, Nano Lett., 15 (7), pp. 4730–4736.

[16] Michalas L. et al., (2015), Modeling and de-embedding the interferometric scanning microwave microscopy by means of dopant profile calibration, Appl. Phys. Lett. 107, 223102.

[17] Farina M. et al., (2011), Calibration Protocol for Broadband Near-Field Microwave Microscopy, IEEE Transactions on Microwave Theory and Techniques, Vol. 59, N. 10, 2769-2776.

[18] Happy H. et al., (2014), Measurement techniques for RF nanoelectronic devices, IEEE Microw. Mag. 1527–3342 30–9.

[19] Trenkler T. et al., (1998), Two-dimensional profiling in silicon using conventional and electrochemical selective etching, J. Vac. Sci. Technol., B: Microelectron. Nanometer Struct., 16, 349.

[20] Schweinböck T. and Hommel S., (2014), Quantitative Scanning Microwave Microscopy: A calibration flow, Microelectronics Reliability, 54(9–10), 2070.

[21] Imtiaz, A. et al., (2012), Frequency-selective contrast on variably doped p-type silicon with a scanning microwave microscope, J. Appl. Phys., 111, 093727.

[22] Eckhardt C. et al., (2010), Geometry effects and frequency dependence in scanning capacitance microscopy on GaAs Schottky and metal–oxide–semiconductor-Type junctions, Physica E: Low-dimensional Systems and Nanostructures, 2/4, pp. 1196-1199.

[23] Smoliner J. et al., (2010), Scanning microwave microscopy/spectroscopy on metal-oxide-semiconductor systems, Journal of Applied Physics, 108 pp. 0643151 – 0643157.